2D Mater.

First principles analysis of the CDW instability of single-layer 1T-$TiSe_2$ and its evolution with charge carrier density

Bogdan Guster[1], Enric Canadell[2], Miguel Pruneda[1], Pablo Ordejón[1]

[1]Catalan Institute of Nanoscience and Nanotechnology (ICN2), CSIC and The Barcelona Institute of Science and Technology, Campus Bellaterra, 08193 Barcelona, Spain
[2]Institut de Ciència de Materials de Barcelona (ICMAB-CSIC), Campus Bellaterra, 08193 Barcelona, Spain

E-mail: pablo.ordejon@icn2.cat

Abstract. We present a Density Functional Theory study of the electronic structure of single-layer $TiSe_2$, and focus on the Charge Density Wave (CDW) instability present on this 2D material. We explain the 2×2 periodicity of the CDW from the phonon band structure of the undistorted crystal, which is unstable under one of the phonon modes at the M point. This can be understood in terms of a partial band gap opening at the Fermi level, which we describe on the basis of the symmetry of the involved crystal orbitals, leading to an energy gain upon the displacement of the atoms following the phonon mode in a 2×1 structure. Furthermore, the combination of the corresponding phonons for the three inequivalent M points of the Brillouin zone leads to the 2×2 distortion characteristic of the CDW state. This leads to a further opening of a full gap, which reduces the energy of the 2×2 structure compared to the 2×1 one of a single M point phonon, and makes the CDW structure the most stable one. We also analyze the effect of charge injection into the layer on the structural instability. We predict that the 2×2 structure only survives for a certain range of doping levels, both for electrons and for holes, as doping reduces the energy gain due to the gap opening. We predict the transition from the commensurate 2×2 distortion to an incommensurate one with increasing wavelength upon increasing the doping level, followed by the appearance of the undistorted 1×1 structure for larger carrier concentrations.

Keywords: Single layer dichalcogenides, charge density waves, density functional theory, titanium diselenide, 2D materials.

1. Introduction

Layered transition-metal dichalcogenides have been the object of large attention for around four decades because they exhibit a rich variety in physical properties [1, 2]. Most notably, these materials have provided a fertile ground for the study of the competition between several electronic instabilities like commensurate and incommensurate charge-density-waves (CDW), superconductivity (SC), etc. A remarkable aspect is that their layered nature makes the alteration of the band filling and the transport properties possible through chemical intercalation. Very recently, the interest in these materials has experienced a sudden resurgence because of the exciting possibility of preparing and studying thin slabs with a reduced number of layers or even single-layers [3, 4]. This makes it possible to study how the reduced electronic screening brought about by lowering the dimensionality from bulk to layers of different thickness influences the competition between electronic instabilities.

1T-$TiSe_2$ holds a special position among the conductive layered transition-metal dichalcogenides in that it is formally a d^0 compound, so that its normal state must be either a semimetal or a semiconductor with a very small gap, a feature that has long been debated [1, 2, 5]. This is in contrast with the situation for most of the other CDW-bearing transition metal dichalcogenides which are formally d^1 compounds like 1T- and 2H-MX_2 (M = Nb, Ta; X = S, Se) and thus exhibit a partially filled conduction band. In addition, neither bulk 1T-TiS_2 nor bulk 1T-$TiTe_2$ exhibit any CDW. However a 2 × 2 CDW has been reported for single-layer 1T-$TiTe_2$ whereas no sign of the instability has been found in bilayers or multilayers. [6] On the basis of DFT calculations it has also been reported an incipient stabilization of the CDW in sheets of 1T-TiS_2 with four or less layers [7].

The bulk structure of 1T-$TiSe_2$ is built from hexagonal layers of Ti atoms in an octahedral coordination (see Fig. 1a) [8]. Short Se-Se contacts occur within the layer but there are also relatively short interlayer Se-Se contacts providing a substantial interlayer coupling. Bulk 1T-$TiSe_2$ exhibits a CDW transition around 200 K which has been controversial for four decades [1, 2, 5, 9, 10, 11, 12, 13, 14, 15]. It leads to a 2 × 2 × 2 commensurate phase (see Fig. 1b) without the occurrence of any intermediate

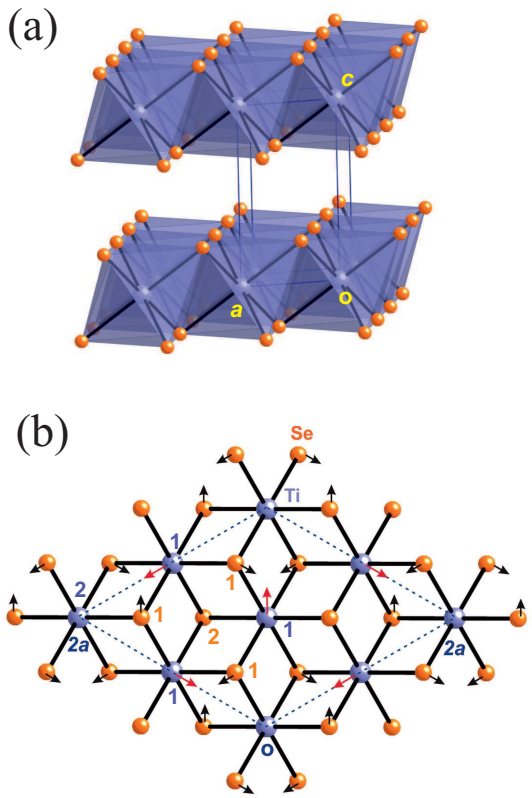

Figure 1. (a) Crystal structure of 1T-$TiSe_2$. (b) Schematic representation of the displacements associated with the CDW in a single-layer of $TiSe_2$.

incommensurate phase [16]. Although 1T-$TiSe_2$ is not superconducting at low temperature, the CDW may be suppressed either by Cu intercalation [17] or applying pressure [18] and under such circumstances superconductivity may be stabilized (maximum T_c = 4.15 K for $Cu_{0.08}TiSe_2$ or 1.8 K at ∼ 3 GPa). On the basis of these observations the possible relationship with the phase diagram of electron doped MoS_2 has been considered [19].

The layered nature of the material as well as the above mentioned interplay between SC and CDW orders in the bulk make 1T-$TiSe_2$ an ideal candidate for studies of the physics associated with these electronic instabilities at the two-dimensional (2D) limit. Recently, a scanning tunneling microscopy (STM) study of single-layer 1T-$TiSe_2$ provided evidence for the existence of a 1×1 structure at room temperature but a 2×2 superstructure at low temperature [20], although

no details about the electronic structure of the single-layers were reported. More recently, two angle-resolved photoemission spectroscopy (ARPES) studies of single-layer 1T-$TiSe_2$ on bilayer graphene (BLG) terminated SiC(001) provided detailed but somewhat conflicting results about the system. For instance, whereas Sugawara *et al* [21] found that the CDW occurs at ~ 200 K, a value very similar to that for bulk 1T-$TiSe_2$ (202 K) and lower than that for exfoliated films with thickness smaller than 100 nm ($\sim$ 240 K), Chen *et al* [22] reported that the CDW temperature is $\sim$ 232 K. The last authors also reported the existence of a small band gap already at room temperature whereas Sugawara *et al* [21] observe an electron pocket at the Brillouin zone (BZ) corner above the CDW. It is possible that electron doping of the samples could be at the origin of some of these seemingly conflicting results. The two studies however agree in suggesting that the CDW is more robust in the single-layer than in bulk. Raman spectra studies showed that the CDW transition temperature increases when moving from the bulk to sheets at the nanometer range although it can decrease for very thin ones probably because of surface oxidation or defects [23, 24].

Let us also note that, because of the existence of Se-Se contacts shorter than the sum of the van der Waals radii, the electronic structure near the Fermi level in bulk and single-layers can be somewhat different, which can have important consequences for a system with either a small semimetallic overlap or a very small semiconducting gap. For instance, the well-known pancake-like hole pocket occurring in bulk for the related 2H-$NbSe_2$ [25] does not occur at all in single-layers of the same material [26]. In addition, because of the observation of the suppression of the CDW under Cu intercalation in bulk 1T-$TiSe_2$, the structural and electronic dependence of the CDW occurrence with the charge-carrier density in single-layers becomes a topic of utmost importance. Recent work with single-crystals of 1T-$TiSe_2$ with thicknesses less than 10 nm, in which the charge carrier density was modified by means of electric field gating, indeed demonstrated a very remarkable phase diagram [27].

There is a considerable number of theoretical studies of the electronic structure of bulk 1T-$TiSe_2$, many of them devoted to the discussion of the origin of the CDW [28, 29, 30, 31, 32, 33, 34, 35, 36]. However, only in more recent works [37, 38] the structural dependence of the electronic and vibrational properties were considered in detail. Fu and coworkers [39] analyzed the effect of doping and biaxial strain on the soft phonons giving rise to the CDW in the bulk. For single-layer 1T-$TiSe_2$ we are aware of only a few theoretical reports. In the earlier one by Fang *et al* [32] the electronic structure was discussed on the basis of the room temperature bulk structure without any type of structural relaxation. In the recent work by Sugawara *et al* [21] the band structure near the Fermi level was calculated for the normal and CDW phase. More recently, Singh *et al* [40] studied the phonon dispersion and showed the presence of an unstable phonon mode but the charge-carrier density dependence of the results was not studied. Yet, in view of the above mentioned recent experimental results the charge-carrier dependence is a truly essential aspect to consider. Chen *et al* [41] looked for dimensional effects on the CDW transition by means of ARPES and DFT calculations on sheets with one to six $TiSe_2$ layers.

In order to provide ground for the discussion and rationalization of the recent exciting results concerning the physics of 1T-$TiSe_2$ at the 2D limit [20, 21, 22, 27], we report here a detailed first-principles DFT study (see the Appendix for computational details) of 1T-$TiSe_2$ single-layers. We will consider in detail the subtleties of the CDW mechanism and how the structural, electronic and vibrational features evolve as a function of the charge-carrier density. From now on we will refer to 1T-$TiSe_2$ simply as $TiSe_2$.

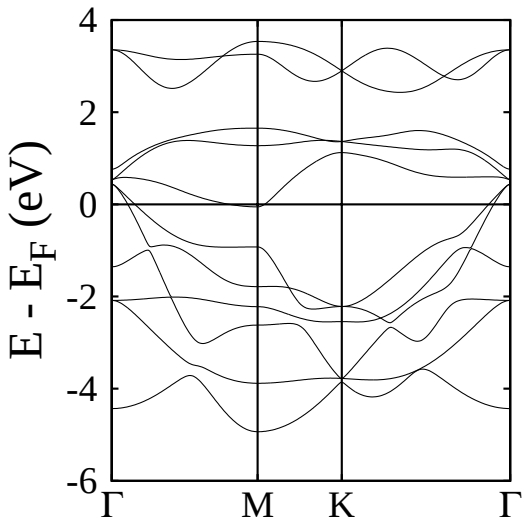

Figure 2. Band structure for undistorted, intrinsic, single-layer $TiSe_2$.

2. Intrinsic single-layer properties

In this Section we discuss the electronic structure and the CDW instability for the free-standing $TiSe_2$ single layer, in the case where there are no externally induced charge carriers. We will refer to it as the *'intrinsic'* case, in contrast with the one in which we consider the presence of externally induced and controlled charge

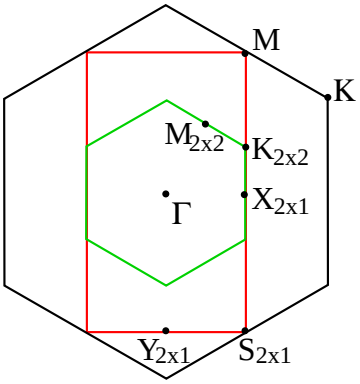

Figure 3. Representation of the Brillouin zone of single-layer $TiSe_2$. Black, red and green show the contours of the BZ of the primitive cell and the 2×1 and 2×2 cells, respectively. The notation of the high symmetry points is also indicated.

carriers, which will be refereed to as the *'doped'* case (although the origin of the charge carriers may not necessarily be the presence of dopant impurities, but other external factors such as electric field gating as in Ref. [27]).

Fig. 2 shows the calculated band structure for the intrinsic, undistorted $TiSe_2$ single-layer. The notation for the high symmetry points (Γ, M and K) of the BZ is indicated in Fig. 3. We obtain a semimetallic behavior, with a 'negative gap' of 0.5 eV between the two bands crossing the Fermi level near the Γ point (which are degenerate at that point in the absence of spin-orbit interactions), and the upper band that has its minimum at the M point. These two sets of bands lead to two pockets of holes around the Γ point and a pocket of electrons around each of the M points of the BZ of the undistorted crystal lattice. Our results are consistent with recent calculations for the single-layer by Chen *et al.* [22], although they find a smaller negative gap of 0.2 eV. This is due to the different DFT functionals used in both calculations: while they use a Heyd-Scuseria-Ernzerhof (HSE) hybrid functional [42] (which usually provides gap energies in good agreement to the experimental data), we use a GGA functional, which tends to underestimate the gap energies (leading in this case to a too large overlap between the two bands, and an overestimated negative gap). A second difference with the results of Chen *et al.* [22] is the splitting of the bands at Γ induced by the spin-orbit coupling term introduced in their calculations, which we do not consider here.

The band leading to the electron pockets at M is an almost exclusively Ti-based band that, at Γ, is built from one of the three t_{2g} orbitals of Ti. In this t_{2g} block, located between 0.5 and 1 eV above the Fermi level, two of the bands are degenerate at Γ and the other one is non-degenerate. Assuming a local coordinate system in which the three-fold symmetry

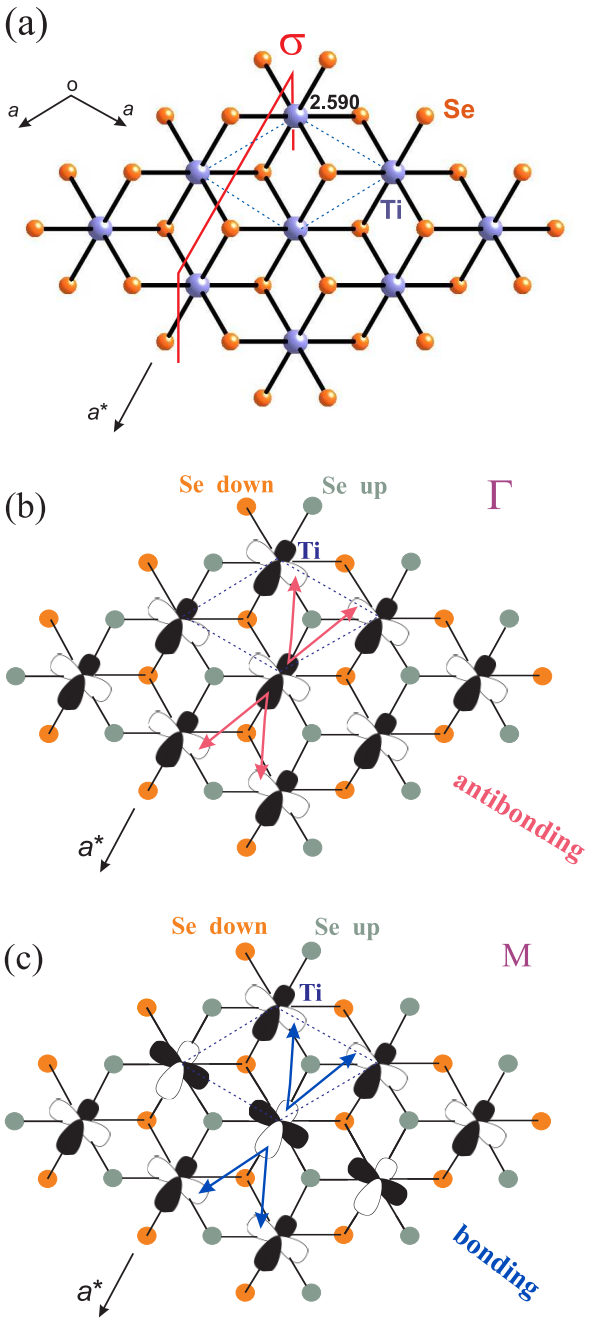

Figure 4. (a) Calculated structure of the undistorted single-layer $TiSe_2$. Orange (blue) circles denote Se (Ti) atoms. In (b) and (c) we show a schematic representation of the crystal orbital of the band leading to the electron pockets for the undistorted single-layer $TiSe_2$ at Γ (b) and M (C). Orange (green) circles denote up (down) Se atoms. The red/blue arrows indicate the antibonding/bonding metal-metal interactions changing from Γ to M. In (a), σ denotes the plane of symmetry preserved by those wave-functions along the $\Gamma - M$ line.

axis of the octahedron occurs along the z direction, the non-degenerated band is essentially built from the Ti d_{z^2} orbital which occurs slightly higher in energy than the doubly-degenerate pair because of the slight rhombohedral distortion. The doubly-degenerate set is mainly built from the Ti $d_{x^2-y^2}$ and d_{xy} orbitals which are somewhat tilted because the plane of the Ti atoms is not a symmetry plane. All the way along the Γ-M line (i.e. along the a^* direction), the only symmetry element preserved is the symmetry plane perpendicular to the layer and going along the a^* direction (the plane noted σ in Fig. 4a). Although at Γ the symmetry is higher, the two doubly-degenerate levels can be described as symmetric and antisymmetric crystal orbitals with respect to this plane. It is the symmetric one (schematically shown in Fig. 4b and Fig. 4c for Γ and M, respectively) which leads to the electron pockets at M. At Γ, such crystal orbital is almost exclusively made of slightly tilted Ti $d_{x^2-y^2}$ orbitals, each of which makes antibonding interactions with those of four nearest-neighbor octahedra (shown by red arrows in Fig. 4b). From Γ to M the phase changes in such a way that these antibonding interactions turn into bonding (see Fig. 4c) and lead to the band dispersion towards higher binding energies. The metal-metal interactions are then responsible for the semi-metallic character of the material, as the dispersion of the Ti $d_{x^2-y^2}$ band is such that it reaches energies around the M point which are below those of the Se-based valence bands which have their maximum at Γ, thus creating the electron and hole pockets centered at M and Γ, respectively. Of course, the same analysis holds for the other equivalent M points in the BZ, with the appropriate Ti d orbital rotations by 120° and 240° around the three-fold symmetry axis.

In order to study the stability of the single-layer, we have performed calculations of the phonon band structure for the optimized, undistorted 1×1 structure. The results are shown in Fig. 5. One of the phonon branches becomes clearly unstable around the M point, similarly to what was found for the bulk crystal [37, 38, 39] for the M and L points of the bulk BZ. The pattern of the distortion associated with the unstable phonon at M is shown schematically in Fig. 6. The displacements of the Ti and Se atoms are perpendicular to the phonon wave vector $\mathbf{q}$. We find that the ratio between the Ti and Se displacements is 3.22, in excellent agreement with the value reported in a recent X-ray study of single-layer $TiSe_2$, 3.3 [43]. It is also very close to that found for the bulk CDW experimentally [16] (3.0±0.9) and from DFT [37] (in the range from 2.3 to 2.9, depending on the choice of the functional and lattice constants). The resulting structure has a 2×1 periodicity: single in the direction of the lattice vector perpendicular to the wave vector $\mathbf{q}$, and double in the direction of the other lattice vector.

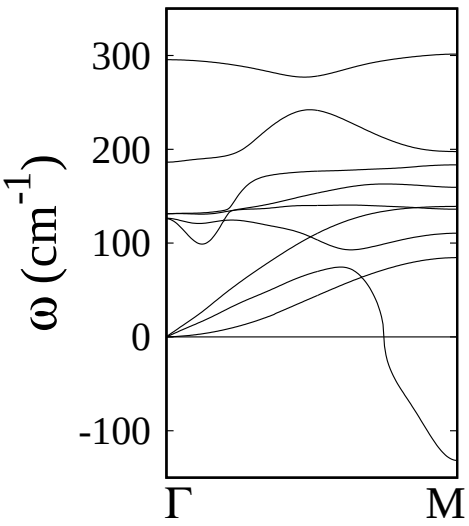

Figure 5. Phonon dispersion for the undistorted, intrinsic, single-layer $TiSe_2$ in the $\Gamma - M$ segment of the BZ.

The presence of phonons with imaginary frequency around the M points indicates that the lattice is unstable against distortions with 2×1 (and symmetry-equivalent) periodicity. This has been confirmed by computing the energy as a function of the amplitude of the phonon mode in a 2×1 supercell. An energy minimum is found, 3 meV per formula unit lower than the undistorted 1×1 structure. A further relaxation in which the 2×1 periodicity is imposed but the internal degrees of freedom are not constrained to follow the unstable phonon mode, produces a negligible energy gain.

The instability of a single M phonon does not lead by itself to the 2×2 CDW distortion pattern. To understand how does the 2×2 CDW structure develops, we notice that, as in the bulk crystal [29, 37], the combination of the three distortions shown in Fig. 6a-c, corresponding to the unstable phonons of the three inequivalent M points, leads to a structure with 2×2 periodicity and precisely the same displacement pattern of the 2×2 CDW shown in Fig. 1b. The energy gained by this triple-q (or $3Q$) combined distortion is 6 meV per formula unit, which is twice as large as that of each individual, single-q (or $1Q$), M phonon distortion with 2×1 periodicity. This is an interesting result, showing that, as in the bulk, the concerted motion combining the three M phonons leads to an enhanced energy gain, with a displacement pattern similar to that of the experimental 2×2 CDW distortion in the bulk.

Fig. 7 shows the relaxed $3Q$, 2×2 distorted single-layer $TiSe_2$ structure, which should be compared with the undistorted 1×1 shown in Fig. 4a. In

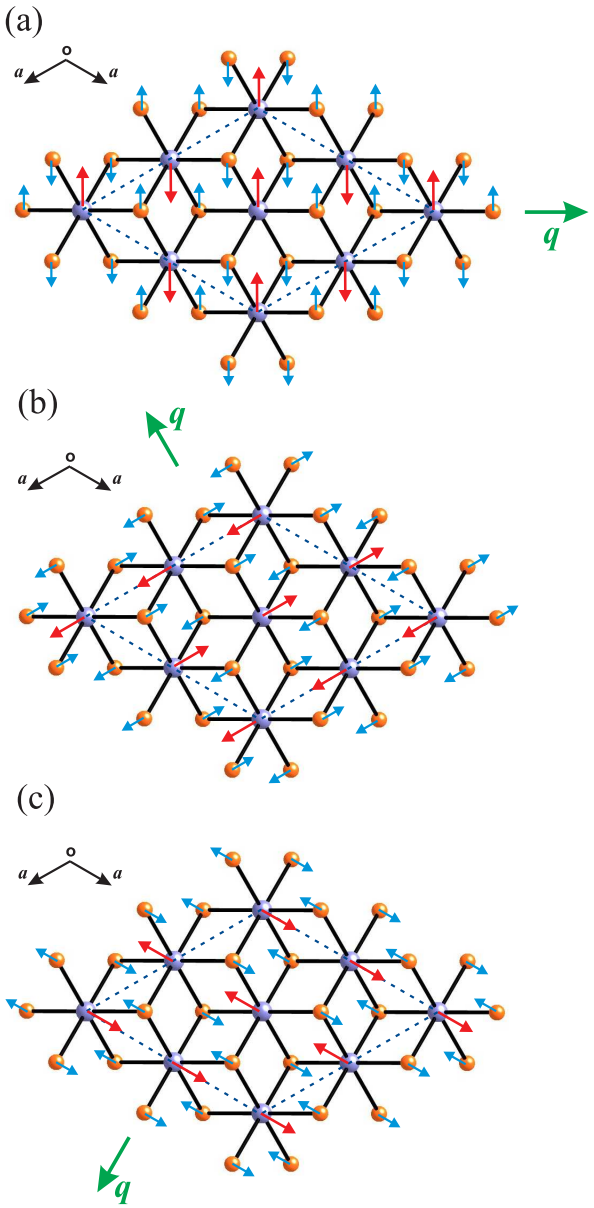

Figure 6. Scheme showing the atomic displacements corresponding to the unstable phonon at the M point (see Fig. 5) for the intrinsic single-layer $TiSe_2$. Each panel shows the displacement pattern for **q** vectors corresponding to the three inequivalent M points of the BZ. The combination of the three modes produces the $3Q$ structural distortion of the 2×2 CDW precisely as shown in Fig. 1b

the undistorted structure there is only one type of octahedra, with the six Ti-Se bonds having identical lengths (2.590 Å) and a small rhombohedral distortion. In the 2×2 distorted structure there are two different types of octahedra (one of type I and three of type II per unit cell). Those at the origin of the 2×2 primitive cell plotted in Fig. 7 (octahedra I) have the six Ti-Se bonds of identical length (2.593 Å) and very similar to those of the undistorted structure. These bonds are shown in black in Fig. 7. Octahedra II have two short,

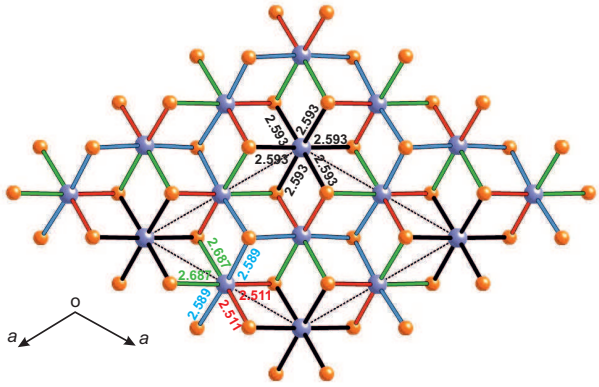

Figure 7. Calculated structure for the 2×2 distorted single-layer $TiSe_2$. The Ti-Se bonds of octahedra I are shown in black; the short(long) bonds in octahedra II are shown in red(green) respectively and the two intermediate ones are shown in blue.

two long and two intermediate Ti-Se bonds which are shown in red, green and blue colors respectively in Fig. 7. Along two of the four-fold axes of the octahedra II (the axes passing though the central Ti atom and the two Se atoms on opposite vertices; these are not true symmetry axes because of the small angular distortions, but we use them as simple descriptors) there is a Se-Ti..Se bond alternation with one bond shorter (2.511 Å) and one bond longer (2.687 Å) than those in the undistorted phase (2.590 Å). Along the third four-fold axis the two bonds are identical (2.589 Å), and very similar to that in the undistorted phase. In turn, every regular octahedron of type I is surrounded by six type II octahedra sharing two Se atoms with the central one in such a way that these two Se atoms are making two short (red) or two long (green) Ti-Se bonds. Consequently, the three-fold symmetry axis going through the Ti atom of the octahedra I is preserved, and an hexagonal lattice is also obtained for the 2×2 distorted single-layer $TiSe_2$.

We now analyze the correlation between the structural distortions of the single layer and the changes in the electronic structure, which is ultimately at the origin of the instability of the undistorted phase. Fig. 8a shows the change in the electronic band structure induced by a $1Q$ distortion. The bands are compared to those of the undistorted lattice, and shown in the BZ of the 2×1 cell. The M point of the 1×1 cell in the direction of the double periodicity is now folded into the Γ point of the 2×1 supercell, and the corresponding electron pockets can now interact with the hole states from Γ, opening some gaps around the Fermi level. However, the S point of the 2×1 supercell coincides with one of the M points of the undistorted cell, as can be seen in Fig. 3 (since one of the original periodicities is maintained), thus still leading to a pocket of electrons at this point of the

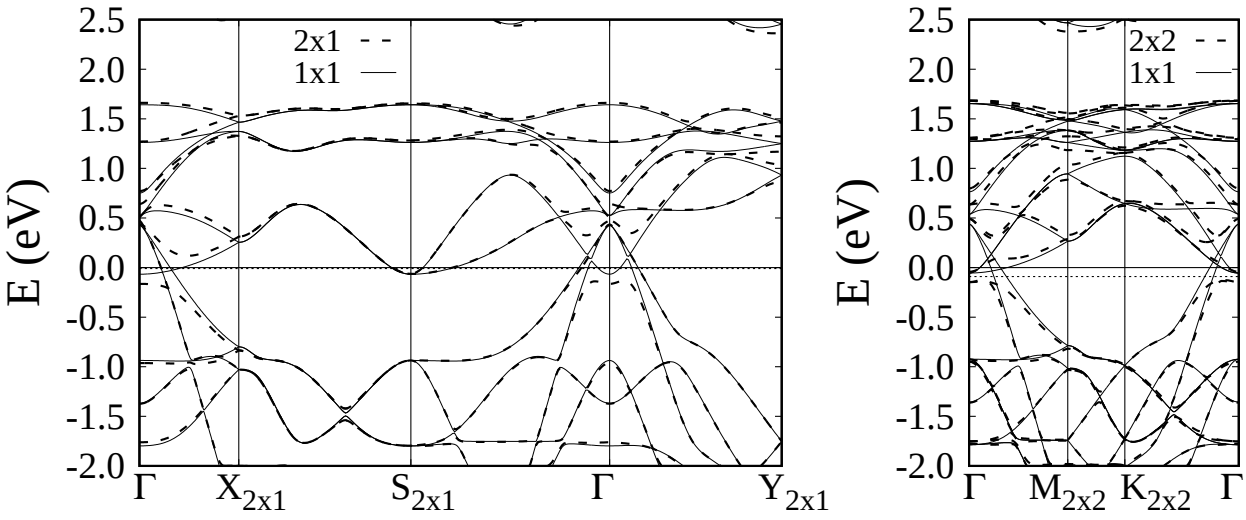

Figure 8. Band structure for the intrinsic single-layer $TiSe_2$. Broken lines correspond to the 2×1 structure corresponding to the displacement of the unstable M phonon (left panel), and for the 2×2 CDW structure (right panel). Full lines show the bands of the 1×1 undistorted structures, respectively. The bands are represented in the BZ of the 2×1 (left) and 2×2 structures (right), and therefore are folded with respect to those shown in Fig. 2. The origin of the energy scale is the Fermi level of the undistorted phase. The Fermi level of the distorted phases is indicated by the dotted horizontal lines.

BZ, and a metallic band crossing the Fermi level near this point (and, correspondingly, a hole pocket and a metallic band at Γ). The $1Q$ distortion therefore reduces the metallic character of the band structure, by splitting some of the bands around the Fermi level, but is not able to open a full gap. This is fully consistent with the symmetry analysis presented above, as the $1Q$ distortion breaks the symmetry with respect to the σ plane. The Ti $d_{x^2-y^2}$ band is practically Ti-Se non-bonding as far as the symmetry plane σ is kept in the structure. However, if the Ti atom moves out of this plane, the symmetry is lost and the Ti and Se orbitals around the Fermi level can effectively mix, thus leading to an energy gain and opening of a gap. In view of the nature of the Ti d orbitals in Fig. 4, the most effective Ti movement to produce such mixing is a displacement perpendicular to the a^* direction, because in that way two Se-Ti..Se bond alternations are produced while leaving the other two Ti-Se bonds barely changed. Such bond alternations are known to be globally stabilizing because the bonding gained in the two red bonds outweighs the bonding lost in the two green ones [31]. This is precisely the type of displacement brought about by the unstable M phonon, as shown in Fig 6

The $3Q$ CDW distortion reduces further the symmetry, as now all the three inequivalent M points of the undistorted BZ fold into Γ, and therefore the bands leading to the three electron pockets can interact with those leading to the hole pockets. The result is that a clean gap opens up now, as shown in Fig. 8b. The full opening of the gap as several M phonons are combined to form the $3Q$ distortion is the reason for the energy gain in of the $3Q$ phase respect to the single-phonon $1Q$ phase. This can be seen clearly in Fig. 9, which compares the electronic density of states (DOS) around the Fermi level for the undistorted layer, and for $1Q$, $2Q$ and $3Q$ distortions (i.e., combining one, two and three inequivalent M phonons). The DOS around E_F decreases as successive phonons are included in the distortion, until a clean gap develops for the $3Q$ CDW. Also, the position of the Fermi level shifts towards lower energies. Both changes lead to the energy stabilization of the CDW phase.

Both the metal-metal interactions which lower the energy of the Ti $d_{x^2-y^2}$ orbitals from Γ to M, and Ti-Se interactions which lead to the gap opening through the mixing allowed by the symmetry breaking, cooperate in providing the energy stabilization produced by the 2×2 modulated structure. This is in contrast with the case of single-layer $1H$-$NbSe_2$ where the driving force for the low temperature 3×3 modulated structure is the optimization of the metal-metal interactions [26].

3. Influence of doping

The injection of charges in the $TiSe_2$ single-layer may have important consequences on its structure and physical properties, as shown by the rich phase diagram under chemical [17] and electrostatic [27] doping. Here, we analyze these effects by introducing extra charges (either positive or negative) explicitly in our DFT calculations. Details are given in Appendix A.

For each value of the doping, we optimize

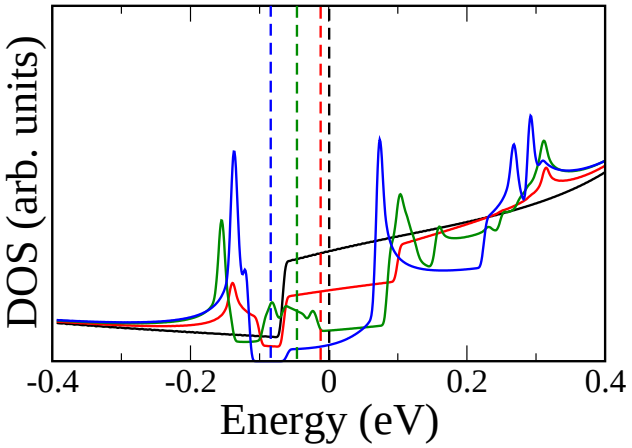

Figure 9. Electronic Density of States for single-layer $TiSe_2$, in the vicinity of the Fermi level. The black curve corresponds to the undistorted structure, while the red, green and blue ones to the 1Q, 2Q and 3Q distorted structures, respectively (see text for details). The position of the Fermi level for each case is shown with a vertical dashed line.

the structure of the undistorted crystal, using the 1×1 periodicity. For the range of doping values considered, we do not see any significant changes in the lattice constant with respect to the undoped case. As a consequence, the positions of the Ti atoms remain unchanged with doping, as well as the in-plane location of the Se atoms. The height of the latter does change with doping, as will be shown below. We then follow the same procedure as for the undoped case, and compute the phonon structure in order to determine the drive towards structural instabilities as a function of doping. The resulting phonon band structures in the Γ-M line are summarized in Fig. 10 for electron (top) and hole doping (bottom), respectively.

For small values of the doping, the phonon spectra are qualitatively similar to the undoped case. In particular, the presence of an unstable mode around the M points of the Brillouin zone is observed. However, the imaginary frequency of this mode evolves significantly with the doping level. The evolution is shown in Fig. 11a. The phonon at M becomes stable at a certain value of the doping, which is around 0.23 and 0.07 $|e|$ per formula unit for electron and hole doping, respectively. For each value of the doping, we have also performed structural relaxations to obtain the distortion of the 2×2 structure. In all cases, we obtain a $3Q$ pattern as the one obtained for the intrinsic layer. Fig. 11b shows the energy difference between the undistorted 1×1 phase and the 2×2 distorted structure as a function of doping. The 2×2 distortion disappears at the same doping values as those for which the M phonon becomes stable.

Fig. 12 present the variation of the structural distortions associated with the $3Q$, 2×2 phase as a function of doping. The in-plane displacements of the Ti and Se atoms following the pattern of Fig. 1b, and the height z of the Se atoms from the plane of the Ti atoms are shown in Figs. 12a and 12b, respectively. For reference, we also include the evolution of the Se height for the non-distorted 1×1 phase, and that of the two types of Se atoms in the 2×2 phase. Again, we observe that the distortions away from the 1×1 symmetry disappear at the same values as the instability of the M phonon.

The mechanism for the stabilization of the 2×2 CDW state in the doped case is the same as in the intrinsic one: the hybridization of the hole and electron pockets allowed by the symmetry breaking, and the consequent opening of a significant band gap around the Fermi level. As we showed before, for the intrinsic case, the Fermi level lays within the gap, making the system a semiconductor. This is imposed by electron counting (as the number of electrons in the system is an integer). For the doped case, the distortion provokes a similar gap in the band structure, but the extra carriers (either electrons or holes) must accommodate within the conduction or valence bands, and the system remains metallic. Nevertheless, for sufficiently small doping values, the distortion still produces a lowering of the energy, driven by the reduction of the DOS near the Fermi level, and the increase of states at lower energies (at the peak defining the band edge). This situation only holds when the doping levels are sufficiently small, so that the Fermi level lays at energies with a significantly modified DOS. A simple model in which the energy gain is estimated from the change of the DOS leads to values of the critical doping for which the 2×2 phase is stable that are quite similar to the ones obtained above, with a difference in a factor of two for the range of stability of electrons and hole doping (not far from the factor of 3 that we obtained in our calculations). As the doping level increases and the Fermi level goes further into the valence or conduction bands, the energy gain due to the distortion is reduced, making the structural distortion progressively less pronounced, until the system recovers the 1×1 periodicity.

It is interesting, however, to realize from Fig. 10 that the evolution of the unstable phonons with doping is more complex than the one just described, which took into account only the behaviour of the M phonon. As the doping level increases, the minimum of the unstable phonon frequency displaces from M to smaller values of $\mathbf{q}$, along the $\Gamma - M$ line. Also, for values of the doping where the M phonon is already stable, there is still an unstable part of the branch, with a minimum at an incommensurate value of $\mathbf{q}$ along the $\Gamma - M$ line, which evolves with the doping value. Ultimately, for larger values of the doping, the whole branch

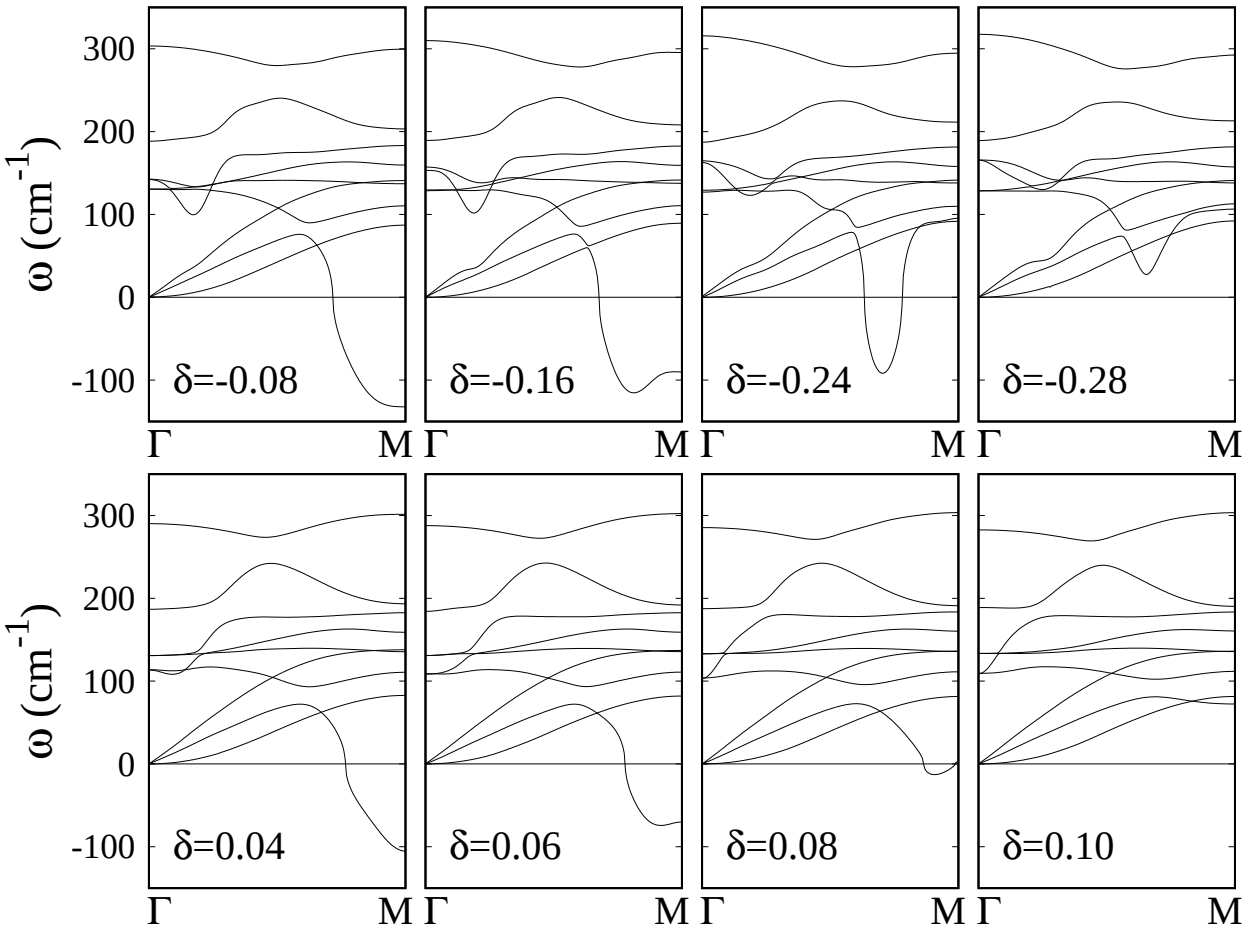

Figure 10. Phonon dispersion for the undistorted single-layer $TiSe_2$ in the $\Gamma - M$ segment of the BZ, for different values of doping δ (in electrons per formula unit). The upper (lower) panels correspond to electron (hole) doping.

becomes stable, as shown in the panels with the largest values of both electron and hole doping in Fig. 10. We expect, therefore, that there will be a transition between a commensurate 2×2 and an incommensurate distortion upon increasing the doping of the layer, until the undistorted 1×1 structure is recovered for sufficiently high doping values The wavelength of the incommensurate distortion is expected to increase for increasing doping values, as the minimum of the imaginary frequency of the unstable phonon shifts towards lower momenta.

4. Conclusions

In summary, a detailed first principles analysis (using Density Functional Theory) has been carried to identify the origin and characteristics of the CDW distortion in single-layer $TiSe_2$. We identify the origin of the 2×2 CDW from the analysis of a phonon branch to becomes stable around the M point of the Brillouin zone. The atomic displacements of this phonon mode allow the mixing of states at the top of the valence band at the Γ point and the bottom of the conduction band at M (both responsible for the metallicity of the undistorted structure), which leads to partial band gap openings that, in turn, lowers the total energy of the system. The combination of three such phonons for the three inequivalent M points allows a full band gap opening and a further energy lowering. This $3Q$ structure has a 2×2 periodicity which closely matches the CDW in-plane distortion of the bulk material.

Doping the layer with externally injected charges modifies this picture only slightly for small doping levels: the energy gain due to the structural distortion is reduced when doping is present, as the Fermi level does not fall at the energy gap opened by the distortion. This makes the atomic displacements and the stabilization energy to decrease with increasing doping level, so that the CDW transition temperature is also expected to decrease, as observed experimentally both in the bulk [17] and in samples of thin layers [27]. Furthermore, our calculations show that, for larger

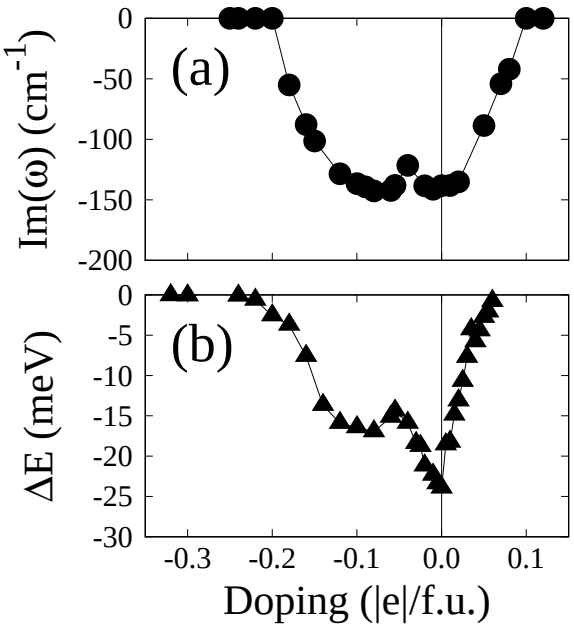

Figure 11. Evolution of the (a) imaginary frequency of the unstable mode at the M point, and (b) the energy decrease due to the 2×2 distortion as a function of the external doping (in electrons per formula unit; negative values indicate electron doping).

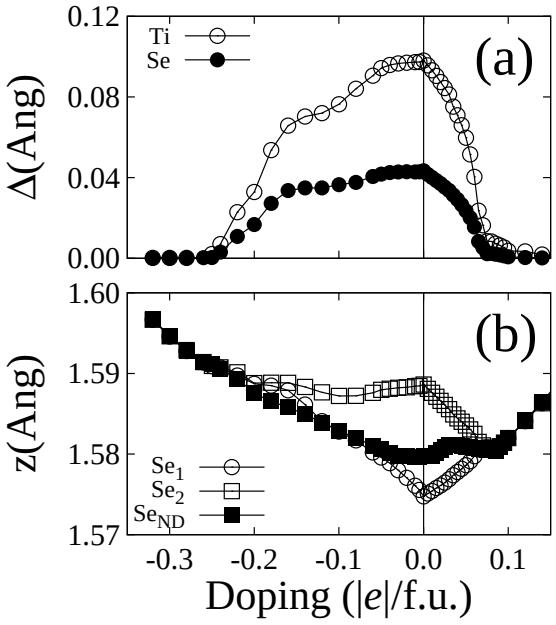

Figure 12. (a) Displacement in the plane parallel to the layer for the Ti and Se atoms from their position in the undistorted phase as a function of doping. (b) Height of the Se atoms as a function of doping. Se_1 and Se_2 correspond to the two inequivalent Se atoms in the 2×2 CDW phase, as shown in Fig. 1. Se_{ND} corresponds to the undistorted, 1×1 phase.

doping levels, the phonon band-structure changes significantly, in such a way that the unstable phonon branch has its minimum at intermediate points of the $\Gamma - M$ segment, while the phonon at M becomes stable. It could therefore be expected that the CDW can become incommensurate for certain values of the doping. Further increase of the doping level makes all the phonon branches to become stable, and therefore the system recovers the undistorted 1×1 structure.

Acknowledgments

This work was supported by Spanish MINECO (Grants FIS2015-64886-C5-3-P and FIS2015-64886-C5-4-P, and the Severo Ochoa Centers of Excellence Program under Grants SEV-2013-0295 and SEV-2015-0496), Generalitat de Catalunya (Grant 2014SGR301 and the CERCA Programme) and by the European Union H2020-EINFRA-5-2015 MaX Center of Excellence (Grant No. 676598).

Appendix A. Computational details

The geometrical optimizations, eletronic and phononic band structures were carried out using a numerical atomic orbitals density functional theory (DFT) [44, 45] approach implemented in the SIESTA code [46, 47]. The Perdew-Burke-Ernzerhof (PBE) functional was used to account for the exchange-correlation energy [48]. The core electrons have been replaced by norm-conserving scalar relativistic pseudopotentials [49] factorized in the Kleinman-Bylander form [50]. We include the $3p$ shell of Ti explicity in the valence, as semicore states. We have used a split-valence double-ζ basis set including polarization functions [51]. The non-linear core-valence exchange-correlation scheme [52] was used for all elements. In the direction normal to the single-layer we chose a vacuum space of 50 Å in order to avoid possible interactions between the layer and its images. In the case of geometrical optimization calculations, the atomic coordinates were relaxed until the forces on them were below 0.004 eV/Å. In all calculations, we use a cutoff of 550 Ry for the real space integrals, and a tolerance of 10^{-5} and 10^{-4} eV on the density matrix ant the total energy, respectively, for the convergence of the SCF cycle. To sample the Brillouin cell for the electronic states, a Monkhorst-Pack [53] k-point grid of 36×36×1 was used for the undistorted minimum cell and it was scaled accordingly where supercell calculations were performed. The phonon band structures were calculated using the finite differences method.

References

[1] Wilson J, Di Salvo F and Mahajan S 1975 *Adv. Phys.* **24** 117–201

[2] Rossnagel K 2011 *J. Phys.:Condens. Matter* **23** 213001

[3] Cao Y, Mishchenko A, Yu G L, Khestanova E, Rooney A P, Prestat E, Kretinin A V, Blake P, Shalom M B, Woods C, Chapman J, Balakrishnan G, Grigorieva I V, Novoselov K S, Piot B A, Potemski M, Watanabe K, Taniguchi T, Haigh S J, Geim A K and Gorbachev R V 2015 *Nano Letters* **15** 4914–4921

[4] Bhimanapati G R, Lin Z, Meunier V, Jung Y, Cha J, Das S, Xiao D, Son Y, Strano M S, Cooper V R, Liang L, Louie S G, Ringe E, Zhou W, Kim S S, Naik R R, Sumpter B G, Terrones H, Xia F, Wang Y, Zhu J, Akinwande D, Alem N, Schuller J A, Schaak R E, Terrones M and Robinson J A 2015 *ACS Nano* **9** 11509–11539

[5] Li G, Hu W Z, Qian D, Hsieh D, Hasan M Z, Morosan E, Cava R J and Wang N L 2007 *Phys. Rev. Lett.* **99** 027404

[6] Chen P, Pai W W, Chan Y H, Takayama A, Xu C Z, Karn A, Hasegawa S, Chou M Y, Mo S K, Fedorov A V and Chiang T C 2017 *Nature Communications* **8** 516

[7] Dolui K and Sanvito S 2016 *EPL* **115** 47001

[8] Riekel C 1976 *J. Solid. State Chem.* **17** 389–392

[9] Anderson O, Karschnick G, Manzke R and Skibowski M 1985 *Solid State Commun.* **53** 339–342

[10] Rossnagel K, Kipp L and Skibowski M 2002 *Phys. Rev. B* **65** 235101

[11] Pillo T, Hayoz J, Berger H, Levy F, L S and Aebi P 2000 *Phys. Rev. B* **61** 16213–16222

[12] Cercellier H, Monney C, Clerc F, Battaglia C, Despont L, Garnier M G, Beck H, Aebi P, Patthey L, Berger H and Forro L 2007 *Phys. Rev. Lett.* **99** 146403

[13] Rohwer T, Hellman S, Wiesenmayer M, Sohrt A, Stangre A, Slomski B, Carr A, Liu Y, Avila L M, Kallane M, Mathias S, Kipp L, Rossnagel K and Bauer M 2011 *Nature (London)* **471** 490

[14] May M M, Brabetz C, Janowitz C and Manzke R 2011 *Phys. Rev. Lett.* **107** 176405

[15] Weber F, Rosenkranz S, Castellan J P, Osborn R, Karapetrov G, Hott R, Heid R, Bohnen K P and Alatas A 2011 *Phys. Rev. Lett.* **107** 266401

[16] Di Salvo F J, Moncton D E and Waszczak J V 1976 *Phys. Rev. B* **14** 4321–4328

[17] Morosan E, Zandbergen H W, Dennis B S, Bos J W G, Onose Y, Klimczuk T, Ramirez A M, Ong N P and Cava R J 2006 *Nature Physics* **2** 544

[18] Kusmartseva A F, Sipos B, Berger H, Forró L and Tutis E 2009 *Phys. Rev. Lett.* **103** 236401

[19] Rösner M, Haas S and Wehling T O 2014 *Phys. Rev. B* **90** 245105

[20] Peng J P, Guan J Q, Zhang H M, Song C L, Wang L, He K, Xue Q K and Ma X C 2015 *Phys. Rev. B* **91** 121113(R)

[21] Sugawara K, Nakata Y, Shimizu R, Han P, Hitosugi T, Sato T and Takahashi T 2016 *ACS Nano* **10** 1341–1345

[22] Chen P, Chan Y H, Fang X Y, Zhang Y, Chou M, Mo S K, Hussain Z, Fedorov A V and T-C C 2015 *Nature Communications* **6** 8943

[23] Duong D L, Ryu G, Hoyer A, Lin C, Burghard M and Kern K 2017 *ACS Nano* **11** 1034–1040

[24] Goli P, Khan J, Wickramaratne D, Lake R K and Balandin A A 2012 *Nano Lett.* **12** 5941–5945

[25] Noat Y, Silva-Guillén J A, Cren T, Cherkez V, Brun C, Pons S, Debontridder F, Roditchev D, Sacks W, Cario L, Ordejón P, García A and Canadell E 2015 *Phys. Rev. B* **92**(13) 134510

[26] Silva-Guillén J A, Ordejón P, Guinea F and Canadell E 2016 *2D Materials* **3** 035028

[27] Li L J, O'Farrell E C T O, Loh K P, Eda G, Özyilmaz B and Castro-Neto A H 2016 *Nature* **529** 185

[28] Zunger A and Freeman A J 1978 *Phys. Rev. B* **17** 1839–1842

[29] Suzuki N, Yamamoto A and Motizuki K 1985 *J. Phys. Soc. Jpn.* **54** 4668–4679

[30] Motizuki K 1986 *Structural Phase Transitions in Layered Transition Metal Compounds* (Reidel: Dordrecht, The Netherlands)

[31] Whangbo M H and Canadell E 1992 *J. Am. Chem. Soc.* **114** 9587–9600

[32] Fang C M, de Groot R A and Haas C 1997 *Phys. Rev. B* **56** 4455–4463

[33] Jishi R A and Alyahyaei H M 2008 *Phys. Rev. B* **78** 144516

[34] Zhu Z, Cheng Y and Schwingenschlögl 2012 *Phys. Rev. B* **85** 245133

[35] Calandra M and Mauri F 2011 *Phys. Rev. Lett.* **106** 196406

[36] Zhu Z, Cheng Y and Schwingenschlögl 2014 *Sci. Rep.* **4** 4025

[37] Bianco R, Calandra M and Mauri F 2015 *Phys. Rev. B* **92** 094107

[38] Duong D L, Burghard M and Schön J C 2015 *Phys. Rev. B* **92** 245131

[39] Fu Z G, Hu Z Y, Yang Y, Lu Y, Zheng F W and Zhang P 2016 *RSC Advances* **6** 76972–76979

[40] Singh B, Hsu C H, Tsai W F, Pereira V M and Lin H 2017 *Phys. Rev. B* **95** 245136

[41] Chen P, Chan Y H, Wong M H, Fang X Y, Chou M Y, Mo S K, Hussain Z, Fedorov A V and Chiang T C 2016 *Nano Lett.* **16** 6331–6336

[42] Heyd J, Scuseria G E and Ernzerhof M 2003 *J. Chem. Phys.* **118** 8207–8215

[43] Fang X F, Hong H, Chen P and Chiang T C 2017 *Phys. Rev. B* **95** 201409(R)

[44] Hohenberg P and Kohn W 1964 *Physical Review* **136** B864–B871

[45] Kohn W and Sham L J 1965 *Physical Review* **140** A1133–A1138

[46] Soler J M, Artacho E, Gale J D, García A, Junquera J, Ordejón P and Sánchez-Portal D 2002 *Journal of Physics: Condensed Matter* **14** 2745–2779

[47] Artacho E, Anglada E, Diéguez O, Gale J D, García A, Junquera J, Martin R M, Ordejón P, Pruneda J M, Sánchez-Portal D and Soler J M 2008 *Journal of Physics: Condensed Matter* **20** 064208

[48] Perdew J P, Burke K and Ernzerhof M 1996 *Physical Review Letters* **77** 3865–3868

[49] Troullier N and Martins J L 1991 *Physical Review B* **43** 1993–2006

[50] Kleinman L and Bylander D M 1982 *Physical Review Letters* **48** 1425–1428

[51] Artacho E, Sánchez-Portal D, Ordejón P, García A and Soler J M 1999 *Physica Status Solidi (b)* **215** 809–817

[52] Louie S G, Froyen S and Cohen M L 1982 *Physical Review B* **26** 1738–1742

[53] Monkhorst H J and Pack J D 1976 *Physical Review B* **13** 5188–5192